Pentavalent iridium pyrochlore $Cd_2Ir_2O_7$: A prototype material system for competing crystalline field and spin-orbit coupling

Jianhong Dai,[1,2] Yunyu Yin,[1,2] Xiao Wang,[1,2] Xudong Shen,[1,2] Zhehong Liu,[1,2] Xubin Ye,[1,2] Jinguang Cheng,[1,2] Changqing Jin,[1,2] Guanghui Zhou,[3] Zhiwei Hu,[4] Shihchang Weng,[5] Xiangang Wan,[6] and Youwen Long[1,2,*]

[1]*Beijing National Laboratory for Condensed Matter Physics, Institute of Physics, Chinese Academy of Sciences, Beijing 100190, China*

[2]*School of Physical Sciences, University of Chinese Academy of Sciences, Beijing 100049, China*

[3]*Department of Physics and Synergetic Innovation Center for Quantum Effects and Applications of Hunan, Hunan Normal University, Changsha 410081, China*

[4]*Max-Planck Institute for Chemical Physics of Solids, Nöthnitzer Straße 40, 01187 Dresden, Germany*

[5]*National Synchrotron Radiation Research Center (NSRRC), 101 Hsin-Ann Road, Hsinchu 30076, Taiwan*

[6]*Department of Physics, Nanjing University, Nanjing 210093, China*

(Received 23 November 2017; revised manuscript received 17 January 2018; published 1 February 2018)

A new pyrochlore oxide $Cd_2Ir_2O_7$ with an Ir^{5+} charge state was prepared by high-pressure techniques. Although strong spin-orbit coupling (SOC) dominates the electronic states in most iridates so that a SOC-Mott state is proposed in Sr_2IrO_4 in the assumption of an undistorted IrO_6 octahedral crystalline field, the strongly distorted one in the current $Cd_2Ir_2O_7$ exhibits a competing interaction with the SOC. Unexpected from a strong SOC limit, $Cd_2Ir_2O_7$ deviates from a nonmagnetic and insulating $J = 0$ ground state. It displays short-range ferromagnetic correlations and metallic electrical transport properties. First-principles calculations well reproduce the experimental observation, revealing the large mixture between the $j_{\rm eff} = 1/2$ and $j_{\rm eff} = 3/2$ bands near the Fermi surface due to the significant distortion of IrO_6 octahedra. This work sheds light on the critical role of a noncubic crystalline field in electronic properties which has been ignored in past studies of $5d$-electron systems.

DOI: 10.1103/PhysRevB.97.085103

I. INTRODUCTION

Transition-metal oxides composed of $5d$ electrons have been attracting much attention due to the competing interactions among the on-site Coulomb repulsion energy U, enhanced spin-orbit coupling λ ($\lambda \propto Z^4$; Z: atomic number), and crystalline electric field energy Δ. The cooperative effects of these interactions may give rise to many intriguing physical properties such as topologic spin liquids and insulators, Weyl semimetals, axion insulators, and even unconventional superconductivity, etc. [1–5]. In the $5d$-electron family, the Ir-based oxides receive most attention. An interesting finding is the SOC-assisted $j_{\rm eff} = 1/2$ Mott state observed in the canted antiferromagnetic insulator Sr_2IrO_4 [6–13]. If one only considers the spatial extension of the d-electron wave function changing from $3d$ to $5d$, a delocalized electronic behavior is expected to occur in the $5d$ system Sr_2IrO_4 with $5d^5$-electron configuration. However, the strong SOC splits the manifold t_{2g} orbitals into a twofold $j_{\rm eff} = 3/2$ band and a single $j_{\rm eff} = 1/2$ band. Since the energy of the former is somewhat lower than that of the latter, the $j_{\rm eff} = 3/2$ band is fully occupied, making the $j_{\rm eff} = 1/2$ band half filled. A moderate U thus can open a Mott gap, leading to the presence of a $j_{\rm eff} = 1/2$ Mott ground state with antiferromagnetic spin ordering [6,7]. Although this scenario is proposed in the assumption of an undistorted cubic IrO_6 octahedral crystalline field, it was frequently used to explain the emergent phenomena occurring in other $5d$- or even $4d$-electron systems, no matter whether the crystalline field is distorted or not. There is therefore a pressing need to examine the validity of this SOC-assisted Mott state in the distorted octahedral coordination environment to avoid the misunderstanding for the intrinsic physical properties.

Following the scenario mentioned above, a nonmagnetic and insulating ground state would be expected to occur in an $Ir^{5+}(5d^4)$ system due to the fully filled $j_{\rm eff} = 3/2$ band and empty $j_{\rm eff} = 1/2$ band, as observed in $NaIrO_3$ [14,15]. However, when the IrO_6 octahedral crystal field considerably deviates from an undistorted cubic one, the proposed $j_{\rm eff} = 3/2, 1/2$ mechanism may encounter a big challenge [16–19]. Actually, the double perovskite $Sr_2YIr^{5+}O_6$ with noncubic crystal field shows evidence for the failed dominance of SOC [17,18]. Unfortunately, since the YO_6 and IrO_6 octahedra are alternatingly distributed in Sr_2YIrO_6 (i.e., the IrO_6 octahedra are not directly connected with each other), one cannot investigate the electronic states of Ir^{5+} by electrical transport measurement. By comparison, the pyrochlore with a general chemical formula of $A_2B_2O_6O'$ provides a desirable system to study the competing interaction between the crystal field and SOC effect. As shown in Fig. 1(a), the pyrochlore has a cubic crystal structure with space group $Fd\text{-}3m$. It builds from $O'A_4$ tetrahedra and corner-sharing BO_6 octahedra along with the [110] direction. The atomic positions of A, B, and O' are all fixed. The only variable is the O_x site, which can change in a relatively large range from 0.3125 to 0.375 [20]. When the $O_x = 0.3125$, the single BO_6 octahedron is rigid. The larger the O_x value is, the larger the BO_6 octahedral distortion. Therefore, we can on the one hand control the crystal field by

*ywlong@iphy.ac.cn

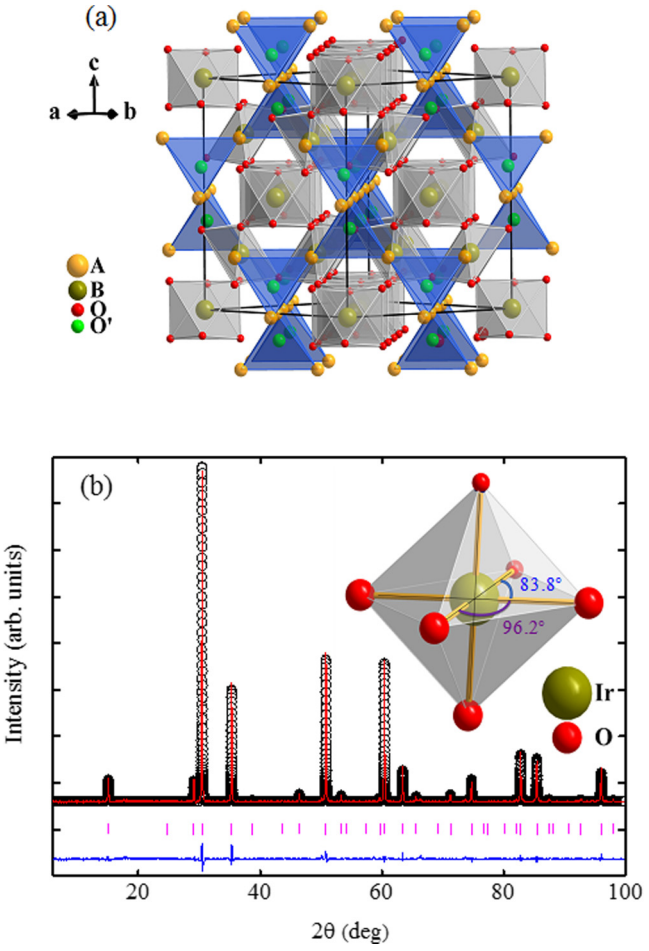

FIG. 1. (a) Crystal structure of pyrochlore with chemical formula $A_2B_2O_6O'$ in space group *Fd-3m*. The $O'A_4$ tetrahedra and corner-sharing BO_6 octahedra are shown. (b) Powder x-ray diffraction pattern and Rietveld refinement results of $Cd_2Ir_2O_7$. Observed (black circle), calculated (red line), and difference (blue line) profiles are shown together with the allowed Bragg reflections (ticks). The inset shows the distorted O-Ir-Or bond angles in a single IrO_6 octahedron.

tuning the atomic position of O_x. On the other hand, we can also measure magnetic and electrical transport properties to characterize the electronic states of Ir ions in the pyrochlore structure. To date the iridium pyrochlore with a pure Ir^{5+} charge state at the *B* site is absent.

In this paper, a novel pyrochlore oxide $Cd_2Ir_2O_7$ with an Ir^{5+} valence state was prepared. Strongly distorted IrO_6 octahedra are observed in this compound. As a consequence, the SOC-dominated nonmagnetic and insulating state expected in a cubic crystal field is found to be invalid in the current distorted one. Instead, the $Cd_2Ir_2O_7$ pyrochlore shows metallic electrical transport and short-range ferromagnetic correlations at low temperature. Moreover, an external magnetic field can upturn the low-temperature resistivity, implying that the field may change the delicate balance between Δ and λ. First-principles calculations are also in agreement with experimental results. Our finding reveals that the effect of a distorted crystal field can play an important role in the intrinsic physics of 5*d*-electron systems.

II. EXPERIMENT AND CALCULATION METHODS

The pyrochlore $Cd_2Ir_2O_7$ was synthesized under high-pressure and high-temperature conditions generated by a cubic anvil-type high-pressure apparatus. Highly pure (>99.9%) CdO, and Ir powders with a 1:1 mole ratio, were used as starting materials, and excessive $KClO_4$ was adopted as an oxidizing agent. The finely mixed reactants were treated at 6.5 GPa and 1373 K for 40 min. The high-pressure product was washed out by de-ionized water to exclude the residual KCl. The phase identification and structural characterization were carried out by powder x-ray diffraction (XRD) using a Huber diffractometer (Cu $K\alpha$ radiation, 40 kV, 300 mA) over a 2θ angle range from 10° to 100° in steps of 0.005°. The GSAS program was used to refine the XRD data based on the Rietveld method [21]. The hard x-ray absorption spectroscopy (XAS) at the Ir-L_3 edge of $Cd_2Ir_2O_7$ together with La_2CoIrO_6 as an Ir^{4+} reference and Sr_2FeIrO_6 as an Ir^{5+} reference were measured in the transmission geometry at the beamline of BL07A at the National Synchrotron Radiation Research Center in Taiwan. Resistivity (ρ) and specific heat (C_p) measurements were performed in a Quantum Design physical property measurement system. Magnetic susceptibility and magnetization were measured on a Quantum Design superconducting quantum interference device magnetometer.

First-principles electronic structure calculations were performed by the local density approximation (LDA) to density functional theory with the full potential, all-electron, linear-muffin-tin-orbital method [22]. Although the 5*d* orbitals are spatially extended, the importance of Coulomb interactions in 5*d* compounds had been confirmed [8]. We used a LDA + U scheme [23] (with $U = 2.0$ eV) to take into account the electron-electron interaction between Ir 5*d* electrons. The crystal structure parameters obtained from the Rietveld refinement in experiment were used for calculations. A $24 \times 24 \times 24$ k mesh was adopted to perform Brillouin zone integration.

III. RESULTS AND DISCUSSION

Figure 1(b) shows the XRD pattern of $Cd_2Ir_2O_7$ measured at room temperature. The Rietveld analysis illustrates that this compound crystallizes into a cubic pyrochlore structure with space group *Fd-3m* (No. 227). The refined structural parameters are listed in Table I. The O_x value in $Cd_2Ir_2O_7$ is found to be 0.329(3), indicating the formation of distorted IrO_6 octahedra. When a single IrO_6 octahedron is examined, the O-Ir-O bond angles in the plane distinctly deviate from 90° while a straight O-Ir-O bonding exists out of the plane [see the inset of Fig. 1(b)]. Furthermore, if one considers the corner-sharing IrO_6 octahedra, the value of the Ir-O-Ir band angle is as small as 132.0°, which is much less than the Y-O-Ir band angle observed in the double perovskite Sr_2YIrO_6 (∼160.3°) mentioned above [17]. These structural features clearly demonstrate the significant octahedral distortion in $Cd_2Ir_2O_7$.

As shown in Table I, the refined Ir-O bond length of $Cd_2Ir_2O_7$ is very close to that observed in Sr_2YIrO_6, suggesting a similar Ir^{5+} valence state in both compounds. To further determine the valence state of Ir, the Ir-L_3 XAS of $Cd_2Ir_2O_7$ and of La_2CoIrO_6 as an Ir^{4+} Ref. [24] and Sr_2FeIrO_6 [25] as

TABLE I. Crystal structural parameters of $Cd_2Ir_2O_7$ obtained from the Rietveld refinement.

Parameter	a (Å)	O_x	Ir-O (Å)	∠Ir-O-Ir (°)	∠O-Ir-O (°)			R_{wp} (%)	R_p (%)
$Cd_2Ir_2O_7$	10.1474(4)	0.329(3)	1.963(4) × 6	132.0(3)	180 × 2	96.19(2) × 2	83.81(2) × 2	4.24	2.88

an Ir^{5+} reference with similar IrO_6 octahedral coordination were measured for comparison. It is well known that the XAS spectra are highly sensitive to the valence state: an increase of the valence state of the metal ion by 1 usually causes a shift of the XAS $L_{2,3}$ spectra by 1 eV or more toward higher energies [26–28]. As shown in Fig. 2, in comparison with the Ir^{4+} reference La_2CoIrO_6, the Ir-L_3 absorption spectrum of $Cd_2Ir_2O_7$ apparently shifts by 1.2 eV to higher energies, but displays a very similar line shape and energy position compared with those of the Ir^{5+} reference Sr_2FeIrO_6, confirming the formation of the Ir^{5+} valence state as well as the oxygen stoichiometry in $Cd_2Ir_2O_7$. This synthesized compound thus provides an iridium pyrochlore composed of a pure Ir^{5+} ionic state at the B site. Note that the oxygen deficient $Pb_2Ir_2O_{6.55}$ was reported to crystallize with a noncentrosymmetric crystal structure [29].

Figure 3(a) shows the temperature dependence of magnetic susceptibility for $Cd_2Ir_2O_7$. One cannot find any long-range spin ordering in the temperature range we measured (2–300 K). Between 8 and 60 K, the magnetic susceptibility can be well fitted by the normalized Curie-Weiss law $\chi = \chi_0 + C/(T - \theta_w)$, giving the temperature-independent term $\chi_0 = 4 \times 10^{-4}$ emu mol^{-1} Oe^{-1} which contains the core diamagnetism and Van Vleck paramagnetism [30–32]. The fitted Curie constant is $C = 0.28$ emu K mol^{-1} Oe^{-1}, and the Weiss constant is $\theta_w = 5.98$ K. According to the Curie constant, the effective magnetic moment is calculated to be $0.75\,\mu_B/Ir^{5+}$. This value is much lower than the spin-only theoretical value ($2.83\,\mu_B$) for an Ir^{5+} ion with $S = 1$, but considerably larger than that obtained for the Ir^{5+} compound $NaIrO_3$, where the SOC-dominated nonmagnetic and insulating behaviors with $J = 0$ are claimed [14]. The positive Weiss constant of $Cd_2Ir_2O_7$ may suggest some short-range ferromagnetic correlations at lower temperatures although we do not find long-range magnetic phase transition with temperature down to 2 K. Figure 3(b) shows the field-dependent magnetization measured at different temperatures. In contrast to the linear magnetization behavior at higher temperatures, the magnetic hysteresis loop is observed at 2 K [see the inset of Fig. 3(b)]. Therefore, the electronic ground state of Ir^{5+} in the current $Cd_2Ir_2O_7$ apparently deviates from the SOC-dominated $J = 0$ state due to the strongly distorted octahedral crystal field. It most probably displays competing SOC and crystal field interaction with comparable λ and Δ values, giving rise to the crossover between the nonmagnetic $J = 0$ state and the spin-ordered $S = 1$ state. Note that the Hund exchange energy is here minor compared with the crystal field energy [33].

Figure 4(a) presents the resistivity as a function of temperature. Essentially different from the insulating conductivity expected for a $J = 0$ state, $Cd_2Ir_2O_7$ shows electrical metallic behavior in the whole temperature region we measured at zero magnetic field. Below 25 K, the resistivity data well follow the Fermi liquid model [see the inset of Fig. 2(b)], suggesting the considerable electronic correlated effects. In the 4d pyrochlore oxides $Pb_2Ru_2O_{6.5}$ and $Bi_2Ru_2O_7$, the metallic electrical behaviors are also observed due to the strong hybridization between the Ru 4d bands and the extended Pb or

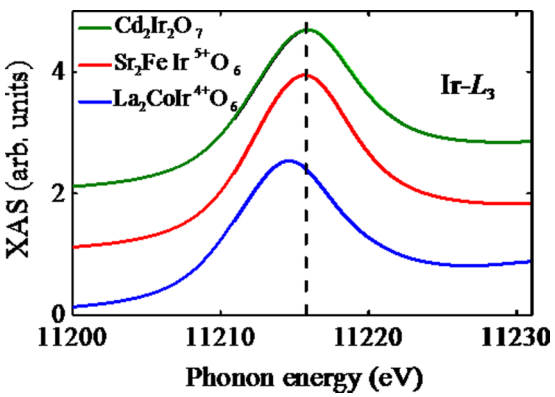

FIG. 2. X-ray absorption spectroscopy of the Ir-L_3 edges of $Cd_2Ir_2O_7$ and the related references for comparison.

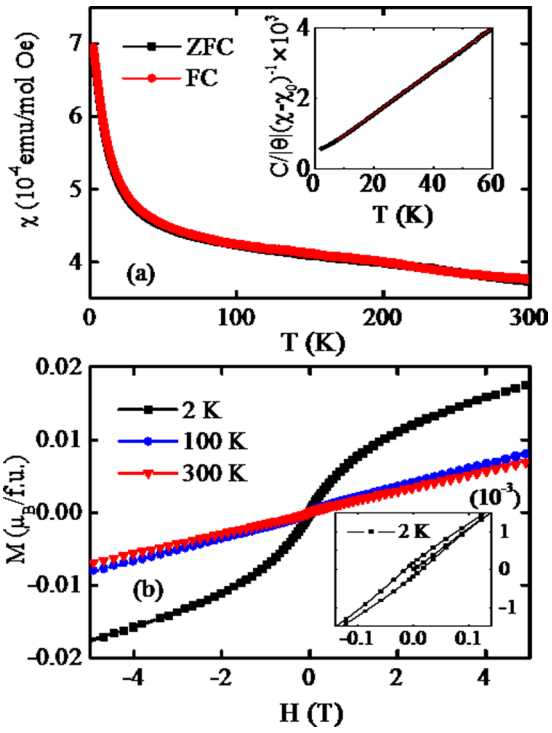

FIG. 3. (a) Temperature dependence of magnetic susceptibility of $Cd_2Ir_2O_7$ measured at 5 T in zero-field-cooling (ZFC) and field-cooling (FC) modes. The inset shows the Curie-Weiss fitting in 8–60 K. (b) Field-dependent magnetization at different temperatures. The inset shows the enlarged view for the magnetic hysteresis behavior at 2 K.

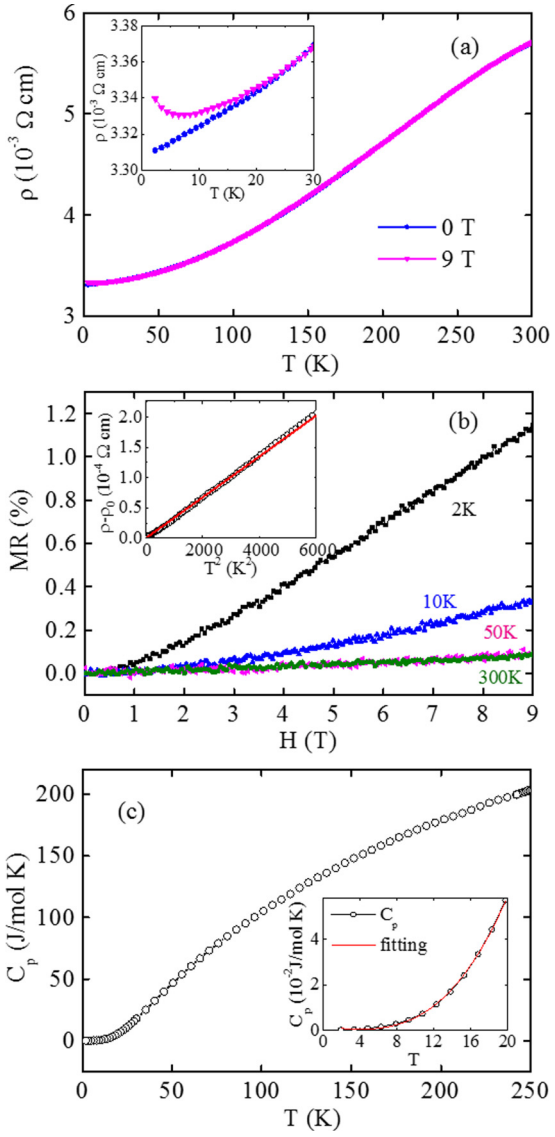

FIG. 4. (a) Temperature dependence of resistivity measured at zero field and 9 T for $Cd_2Ir_2O_7$. The inset shows the enlarged view for field-induced upturn at lower temperatures. (b) Field-dependent magnetoresistance MR ($=100\% \times [\rho(H) - \rho(0)]/\rho(0)$) at different temperatures. The inset shows the resistivity fitted using a Fermi liquid model below 25 K. (c) Specific heat as a function of temperature below 250 K measured at zero field. The inset shows the fitting below 20 K as described in the text.

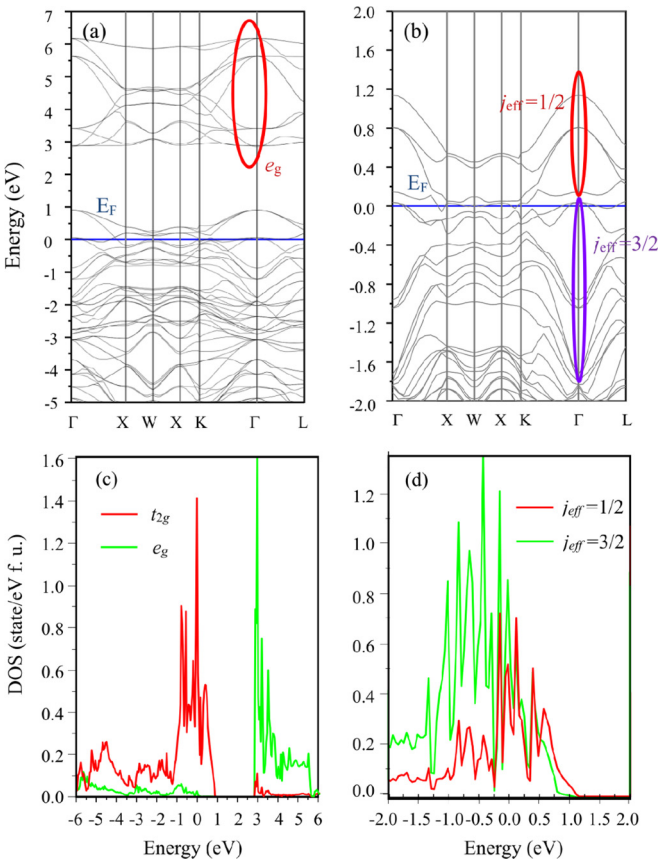

FIG. 5. (a), (b) First-principles numerical results for the band dispersion along several high-symmetry directions of $Cd_2Ir_2O_7$ based on LDA and LDA + SOC methods, respectively. (c), (d) The calculated density of states near the Fermi surface using the LDA and LDA + SOC methods, respectively. One can find strong mixture between the $j_{\text{eff}} = 1/2$ and $3/2$ bands near the Fermi level in (d), indicating the competing Δ and λ.

Bi $6p$ bands [34]. In the present $Cd_2Ir_2O_7$, the $5dt_{2g}$ orbitals of Ir^{5+} dominate the Fermi surface with negligible contribution from the A-site Cd^{2+} (see theoretical calculation results shown later). Therefore, the $5d$-electron hopping via the Ir-O-Ir pathways should be mainly responsible for the metallicity of $Cd_2Ir_2O_7$ [4,33]. More interestingly, if a higher magnetic field (e.g., 9 T) is applied, one can find a rapid upturn in resistivity at lower temperatures, leading to a metal-insulator-like transition as presented in the inset of Fig. 4(a). Since magnetic field can significantly affect the spin-orbit nature [35], the resistivity upturn implies that applying an external magnetic field may change the delicate balance between the competing crystal field and the SOC effect in $Cd_2Ir_2O_7$. Moreover, when the field dependence of resistivity is measured as shown in Fig. 4(b), we find positive and almost linear magnetoresistance behavior above 50 K. At lower temperatures (e.g., at 2 and 10 K), however, a positive curvature is induced by the field.

In accordance with the absence of long-range spin ordering, no specific heat anomaly is observed in $Cd_2Ir_2O_7$ as shown in Fig. 4(c). The low-temperature heat capacity data can be well fitted on the basis of the function $C_p/T = \gamma + \alpha T^2 + \beta T^{1/2}$, yielding $\gamma = 1.22\,\text{mJ/mol K}^2$, $\alpha = 0.62\,\text{mJ/mol K}^4$, and $\beta = 0.272\,\text{mJ/mol K}^{2.5}$. The presence of the γ coefficient is consistent with the metallic conductivity. The significant contribution from the $T^{3/2}$ term suggests some short-range ferromagnetic excitations as expected from magnetization measurement at low temperature. The electrical transport and heat capacity measurements thus further confirm the $J \neq 0$ metallic and short-range ferromagnetic behaviors in $Cd_2Ir_2O_7$ due to the strong noncubic crystal field effect which is comparable with the interaction of SOC.

To get deeper insights into the electronic properties of this rare Ir^{5+} pyrochlore $Cd_2Ir_2O_7$, we performed first-principles density functional theory calculations. Figure 5 shows the band dispersion along several high-symmetry directions as well as

the density of states (DOS) near the Fermi surface. The single Ir atom is octahedrally coordinated by six O atoms, making the Ir-5*d* bands split into the t_{2g} and e_g states. Due to the extended nature of 5*d* states, the splitting between t_{2g} and e_g states is rather large. As shown in Figs. 5(a) and 5(c), the LDA calculations illustrate that the Ir-e_g states distribute from 2.0 to 6.0 eV while the Ir-t_{2g} states locate around the Fermi level. When the SOC is included for calculations, it significantly affects the band dispersion around the Fermi level as presented in Fig. 5(b). The top four bands can be assigned as $j_{\rm eff} = 1/2$ states. However, due to the distortion of IrO_6 octahedra, the mixture between $j_{\rm eff} = 1/2$ and $j_{\rm eff} = 3/2$ bands is quite large. If we plot the DOS as a function of energy near the Fermi surface as shown in Fig. 5(d), this mixture can be seen unambiguously. This is in sharp contrast to the isolated $j_{\rm eff} = 1/2$ and 3/2 bands observed in Sr_2IrO_4 without considering the octahedral distortion. In order to consider the electronic correlation in Ir-5*d* states, we also carried out LDA + U and LDA + U + SOC calculations with U = 2.0 eV. The introduction of U does not change the electronic band structures significantly. To further investigate the magnetism, LDA + U + SOC calculations were carried out for several typical collinear and noncollinear magnetic structures as found in other pyrochlore compounds [4,36]. Our numerical calculations give the saturated magnetic moment to be about 0.05 μ_B/Ir, which again shows the importance of the distorted crystal field in this oxide. For Ir^{4+} pyrochlore oxides, the ground-state magnetic configuration is all in or all out and the net magnetic moment is zero [4], while for the present Ir^{5+} pyrochlore compound the energy discrepancy between different magnetic configurations is very small and consistent with the magnetic moment observed in magnetization measurements.

IV. CONCLUSION

In summary, a new oxide $Cd_2Ir_2O_7$ was successfully synthesized; it is an iridium pyrochlore with a pure Ir^{5+} charge state. Different from most perovskite-type oxides, the current $Cd_2Ir_2O_7$ pyrochlore with corner-sharing IrO_6 octahedra is strongly distorted, providing a desirable prototype material system to study the competing crystalline field and spin-orbit coupling. The expected $J = 0$ ground state in the strong SOC limit is out of work in $Cd_2Ir_2O_7$ because of the significant noncubic crystal field effect which is comparable with the magnitude of SOC. As a result, $Cd_2Ir_2O_7$ shows short-range ferromagnetic correlations and metallic electrical transport features, essentially deviating from the nonmagnetic and insulating $J = 0$ state. First-principles calculations further reveal that due to the strong octahedral distortion of IrO_6, the $j_{\rm eff} = 1/2$ and $j_{\rm eff} = 3/2$ bands are mixed together considerably around the Fermi level, further revealing the nature of the $J \neq 0$ state duo to the competing Δ and λ. We claim that, in addition to the strong spin-orbit coupling, it is also necessary to consider the effect of the distorted crystalline field to fully understand the intrinsic physics of 5*d*-electron systems. Note that Agrestini *et al.* recently reported that the large covalency of iridium in Sr_2IrO_4 can affect the electronic behaviors [37]. The covalent effect may also exist in the present $Cd_2Ir_2O_7$. However, since the pyrochlore $Cd_2Ir_2O_7$ shows much more IrO_6 octahedral distortion compared with that of perovskite-related iridates, we emphasize here the effect of the distorted crystalline field on the $J \neq 0$ electronic states.

ACKNOWLEDGMENTS

This work was supported by the National Natural Science Foundation of China (Grants No. 11574378 and No. 51772324), 973 Project of the Ministry of Science and Technology of China (Grant No. 2014CB921500), and the Chinese Academy of Sciences (Grants No. YZ201555, No. QYZDB-SSW-SLH013, No. XDB07030300, and No. GJHZ1773). The research in Dresden was supported by the Deutsche Forschungsgemeinschaft through SFB 1143.

[1] M. Z. Hasan and C. L. Kane, Rev. Mod. Phys. **82**, 3045 (2010).
[2] A. Shitade, H. Katsura, J. Kunes, X. L. Qi, S. C. Zhang, and N. Nagaosa, Phys. Rev. Lett. **102**, 256403 (2009).
[3] C. H. Kim, H. S. Kim, H. Jeong, H. Jin, and J. Yu, Phys. Rev. Lett. **108**, 106401 (2012).
[4] X. Wan, A. M. Turner, A. Vishwanath, and S. Y. Savrasov, Phys. Rev. B **83**, 205101 (2011).
[5] M. Hajialamdari, F. S. Razavi, D. A. Crandles, R. K. Kremer, and M. Reedyk, J. Phys.: Condens. Matter **24**, 505701 (2012).
[6] B. J. Kim, H. Jin, S. J. Moon, J.-Y. Kim, B.-G. Park, C. S. Leem, J. Yu, T. W. Noh, C. Kim, S.-J. Oh, J.-H. Park, V. Durairaj, G. Cao, and E. Rotenberg, Phys. Rev. Lett. **101**, 076402 (2008).
[7] S. J. Moon, H. Jin, W. S. Choi, J. S. Lee, S. S. A. Seo, J. Yu, G. Cao, T. W. Noh, and Y. S. Lee, Phys. Rev. B **80**, 195110 (2009).
[8] B. J. Kim, H. Ohsumi, T. Komesu, S. Sakai, T. Morita, H. Takagi, and T. Arima, Science **323**, 1329 (2009).
[9] Q. Huang, J. L. Soubeyroux, O. Chmaissem, I. Natali Sora, A. Santoro, R. J. Cava, J. J. Krajewski, and J. W. F. Peck, J. Solid State Chem. **112**, 355 (1994).
[10] M. Ge, T. F. Qi, O. B. Korneta, D. E. De Long, P. Schlottmann, W. P. Crummett, and G. Cao, Phys. Rev. B **84**, 100402(R) (2011).
[11] C. Dhital, T. Hogan, Z. Yamani, C. de la Cruz, X. Chen, S. Khadka, Z. Ren, and S. D. Wilson, Phys. Rev. B **87**, 144405 (2013).
[12] M. K. Crawford, M. A. Subramanian, R. L. Harlow, J. A. Fernandez-Baca, Z. R. Wang, and D. C. Johnston, Phys. Rev. B **49**, 9198 (1994).
[13] S. Fujiyama, H. Ohsumi, T. Komesu, J. Matsuno, B. J. Kim, M. Takata, T. Arima, and H. Takagi, Phys. Rev. Lett. **108**, 247212 (2012).
[14] M. Bremholm, S. E. Dutton, P. W. Stephens, and R. J. Cava, J. Solid State Chem. **184**, 601 (2011).
[15] L. Du, X. Sheng, H. Weng, and X. Dai, Europhys. Lett. **101**, 27003 (2013).
[16] M. M. Sala, K. Ohgushi, A. Al-Zein, Y. Hirata, G. Monaco, and M. Krisch, Phys. Rev. Lett. **112**, 176402 (2014).
[17] G. Cao, T. F. Qi, L. Li, J. Terzic, S. J. Yuan, L. E. DeLong, G. Murthy, and R. K. Kaul, Phys. Rev. Lett. **112**, 056402 (2014).

[18] S. Bhowal, S. Baidya, I. Dasgupta, and T. Saha-Dasgupta, Phys. Rev. B **92**, 121113(R) (2015).
[19] S. Kanungo, K. Mogare, B. Yan, M. Reehuis, A. Hoser, C. Felser, and M. Jansen, Phys. Rev. B **93**, 245148 (2016).
[20] M. A. Subramanian, G. Aravamudan, and G. V. Subba Rao, Prog. Solid State Chem. **15**, 55 (1983).
[21] A. C. Larson and R. B. Von Dreele, General structure analysis system (GSAS), Report No. LAUR 86-748 (Los Alamos National Laboratory, Los Alamos, NM, 1994).
[22] S. Y. Savrasov, Phys. Rev. B **54**, 16470 (1996).
[23] V. I. Anisimov, F. Aryasetiawan, and A. I. Lichtenstein, J. Phys.: Condens. Matter **9**, 767 (1997).
[24] J. Song, B. Zhao, L. Yin, Y. Qin, J. Zhou, D. Wang, W. Song, and Y. Sun, Dalton Trans. **46**, 11691 (2017).
[25] P. D. Battle, G. R. Blake, T. C. Gibb, and J. F. Vente, J. Solid State Chem. **145**, 541 (1999).
[26] R. K. Sahu, Z. Hu, M. L. Rao, S. S. Manoharan, T. Schmidt, B. Richter, M. Knupfer, M. Golden, J. Fink, and C. M. Schneider, Phys. Rev. B **66**, 144415 (2002).
[27] Y. Sakai, J. Y. Yang, R. Z. Yu, H. Hojo, I. Yamada, P. Miao, S. Lee, S. Torii, T. Kamiyama, M. Ležaić, G. Bihlmayer, M. Mizumaki, J. Komiyama, T. Mizokawa, H. Yamamoto, T. Nishikubo, Y. Hattori, K. Oka, Y. Y. Yin, J. H. Dai *et al.*, J. Am. Chem. Soc. **139**, 4574 (2017).
[28] H. S. Deng, M. Liu, J. H. Dai, Z. W. Hu, C. Kuo, Y. Y. Yin, J. Y. Yang, X. Wang, Q. Zhao, Y. J. Xu, Z. M. Fu, J. W. Cai, H. Z. Guo, K. J. Jin, T. Pi, Y. Soo, G. H. Zhou, J. G. Cheng, K. Chen, P. Ohresser *et al.*, Phys. Rev. B **94**, 024414 (2016).
[29] Y. Hirata, M. Nakajima, Y. Nomura, H. Tajima, Y. Matsushita, K. Asoh, Y. Kiuchi, A. G. Eguiluz, R. Arita, T. Suemoto, and K. Ohgushi, Phys. Rev. Lett. **110**, 187402 (2013).
[30] G. Khaliullin, Phys. Rev. Lett. **111**, 197201 (2013).
[31] T. Dey, A. Maljuk, D. V. Efremov, O. Kataeva, S. Gass, C. G. F. Blum, F. Steckel, D. Gruner, T. Ritschel, A. U. B. Wolter, J. Geck, C. Hess, K. Koepernik, J. van den Brink, S. Wurmehl, and B. Büchner, Phys. Rev. B **93**, 014434 (2016).
[32] P. W. Selwood, *Magnetochemistry* (Interscience, New York, 1956).
[33] D. Pesin and L. Balents, Nat. Phys. **6**, 376 (2010).
[34] M. Tachibana, Y. Kohama, T. Shimoyama, A. Harada, T. Taniyama, M. Itoh, H. Kawaji, and T. Atake, Phys. Rev. B **73**, 193107 (2006).
[35] V. Granata, L. Capogna, F. Forte, M. B. Lepetit, R. Fittipaldi, A. Stunault, M. Cuoco, and A. Vecchione, Phys. Rev. B **93**, 115128 (2016).
[36] X. Wan, A. Vishwanath, and S. Y. Savrasov, Phys. Rev. Lett. **108**, 146601 (2012).
[37] S. Agrestini, C.-Y. Kuo, M. Moretti Sala, Z. Hu, D. Kasinathan, K.-T. Ko, P. Glatzel, M. Rossi, J.-D. Cafun, K. O. Kvashnina, A. Matsumoto, T. Takayama, H. Takagi, L. H. Tjeng, and M. W. Haverkort, Phys. Rev. B **95**, 205123 (2017).